10.1098/rsta.2001.0955

THE ROYAL SOCIETY

Multiple-relaxation-time lattice Boltzmann models in three dimensions

By Dominique d'Humières[1], Irina Ginzburg[2], Manfred Krafczyk[3]†, Pierre Lallemand[4] and Li-Shi Luo[5]

[1]*Laboratoire de Physique Statistique, École Normale Supérieure, 24 Rue Lhomond, 75231 Paris Cédex 05, France* (dominique.dHumieres@lps.ens.fr)

[2]*Fraunhofer-Institut für Techno- und Wirtschaftsmathematik, Gottlieb-Daimler-Straße 49, D-67663 Kaiserslautern, Germany* (ginzburg@itwm.uni-kl.de)

[3]*Lehrstuhl für Bauinformatik, Fakultät für Bauingenieur- und Vermessungswesen, Technische Universität München, Arcisstraße 21, D-80290 München, Germany*

[4]*Laboratoire Applications Scientifiques du Calcul Intensif (ASCI), Bâtiment 506, Université Paris-Sud (Paris XI Orsay), 91405 Orsay Cédex, France* (alleman@asci.fr)

[5]*ICASE, Mail Stop 132C, NASA Langley Research Center, Building 1152, 3 West Reid Street, Hampton, VA 23681-2199, USA* (luo@icase.edu)

Published online 12 February 2002

This article provides a concise exposition of the multiple-relaxation-time lattice Boltzmann equation, with examples of 15-velocity and 19-velocity models in three dimensions. Simulation of a diagonally lid-driven cavity flow in three dimensions at $Re = 500$ and 2000 is performed. The results clearly demonstrate the superior numerical stability of the multiple-relaxation-time lattice Boltzmann equation over the popular lattice Bhatnagar–Gross–Krook equation.

Keywords: multiple-relaxation-time LBE in three dimensions; D3Q15 and D3Q19 models; three-dimensional diagonal lid-driven cavity flow

1. Introduction

The relaxation lattice Boltzmann equation (RLBE) was introduced by Higuera & Jiménez (1989) to overcome some drawbacks of lattice-gas automata (LGA) such as large statistical noise, limited range of physical parameters, non-Galilean invariance, and implementation difficulty in three dimensions. In the original RLBE the equilibrium distribution functions and the relaxation matrix were derived from the underlying LGA models. It was soon realized that the connection to the LGA model could be abandoned and the equilibria and collision matrices could be constructed independently to better suit numerical applications (Higuera *et al*. 1989).

The simplest lattice Boltzmann equation (LBE) is the lattice Bhatnagar–Gross–Krook (BGK) equation, based on a single-relaxation-time approximation (Bhatnagar *et al*. 1954). Due to its extreme simplicity, the lattice BGK (LBGK) equation (Qian

† Present address: Institut für Computeranwendungen im Bauingenieurwesen, Technische Universität Braunscweig, Pockelsstraße 3, D-38106 Braunschweig, Germany (kraft@cab.bau.tu-bs.de).

et al. 1992; Chen *et al*. 1992) has become the most popular lattice Boltzmann model, in spite of its well-known deficiencies.

The multiple-relaxation-time (MRT) lattice Boltzmann equation was also developed at the same time (d'Humières 1992). The MRT lattice Boltzmann equation (also referred to as the generalized lattice Boltzmann equation (GLBE) or the moment method) overcomes some obvious defects of the LBGK model, such as fixed Prandtl number ($Pr = 1$ for the BGK model) and fixed ratio between the kinematic and bulk viscosities. The MRT lattice Boltzmann equation has been persistently pursued, and much progress has been made. Successes include formulation of optimal boundary conditions (Ginzbourg & Adler 1994; Ladd 1994), interface conditions in multiphase flows (Ginzbourg & Adler 1995) and free surfaces (Ginzburg & Steiner 2002), thermal (McNamara *et al*. 1995) and viscoelastic models (Giraud *et al*. 1997, 1998), models with reduced lattice symmetries (d'Humières *et al*. 2001; Bouzidi *et al*. 2001*a*), and improvement of numerical stability (Lallemand & Luo 2000). It should be stressed that most of the above results cannot be obtained with the LBGK models. Applying optimization techniques in coding, the computational efficiency of the RLBE method (d'Humières 1992) can be fairly close to that of the LBGK method for most practical applications (RLBE schemes could be *ca*. 15% slower than their LBGK counterparts in terms of the number of sites updated per second). Recently, it was shown that the MRT LBE models are much more stable than their LBGK counterparts (Lallemand & Luo 2000), because the different relaxation times can be individually tuned to achieve 'optimal' stability.

In this paper we intend to bring attention to the MRT LBE by demonstrating its superior stability to LBGK models. This paper is organized as follows. Section 2 briefly outlines the basic theory of the MRT LBE. Section 3 provides as a 'template' example: a 15-velocity RLBE model in three dimensions (D3Q15 model). Section 4 gives some results for a three-dimensional cavity flow simulated by using both RLBE and LBGK methods. Section 5 concludes the paper. The appendix briefly describes the 19-velocity model in three dimensions (D3Q19 model).

2. Multiple-relaxation-time lattice Boltzmann equation

Although it can be shown that the lattice Boltzmann equation is a finite-difference form of the linearized continuous Boltzmann equation (He & Luo 1997*a*, *b*), we present the RLBE as a self-contained mathematical object representing a dynamical system with a finite number of moments in discrete space and time.

The general RLBE model has three components. The first component is discrete phase space defined by a regular lattice in D dimensions together with a set of *judiciously chosen* discrete velocities $\{\boldsymbol{e}_\alpha \mid \alpha = 0, 1, \ldots, N\}$ connecting each lattice site to some of its neighbours. The fundamental object in the theory is the set of velocity distribution functions $\{f_\alpha \mid \alpha = 0, 1, \ldots, N\}$ defined on each node $\boldsymbol{r}_i$ of the lattice. The second component includes a collision matrix $\boldsymbol{S}$ and $(N + 1)$ equilibrium distribution functions $\{f_\alpha^{(\mathrm{eq})} \mid \alpha = 0, 1, \ldots, N\}$. The equilibrium distribution functions are functions of the local conserved quantities. The third component is the evolution equation in discrete time $t_n = n\delta t$, $n = 0, 1, \ldots,$

$$|f(\boldsymbol{r}_i + \boldsymbol{e}_\alpha \delta t, t + \delta t)\rangle - |f(\boldsymbol{r}_i, t)\rangle = -\boldsymbol{S}[|f(\boldsymbol{r}_i, t)\rangle - |f^{(\mathrm{eq})}(\boldsymbol{r}_i, t)\rangle]. \tag{2.1}$$

In the above equation we have used the following notation for column vectors in

$(N+1)$-dimensional space $\mathbb{V} = \mathbb{R}^{N+1}$,

$$|f(\boldsymbol{r}_i,t)\rangle \equiv (f_0(\boldsymbol{r}_i,t), f_1(\boldsymbol{r}_i,t), \ldots, f_N(\boldsymbol{r}_i,t))^{\mathrm{T}},$$
$$|f^{(\mathrm{eq})}(\boldsymbol{r}_i,t)\rangle \equiv (f_0^{(\mathrm{eq})}(\boldsymbol{r}_i,t), f_1^{(\mathrm{eq})}(\boldsymbol{r}_i,t), \ldots, f_N^{(\mathrm{eq})}(\boldsymbol{r}_i,t))^{\mathrm{T}},$$
$$|f(\boldsymbol{r}_i+\boldsymbol{e}_\alpha\delta t, t+\delta t)\rangle \equiv (f_0(\boldsymbol{r}_i,t+\delta t), \ldots, f_N(\boldsymbol{r}_i+\boldsymbol{e}_N\delta t, t+\delta t))^{\mathrm{T}},$$

where the superscript 'T' denotes the transpose operator and we always assume that $\boldsymbol{e}_0 \equiv \boldsymbol{0}$. From here on the Dirac notations of bra $\langle\cdot|$ and ket $|\cdot\rangle$ vectors are used to denote, respectively, the row and column vectors. Note that equation (2.1) is written in such a way that its right- and left-hand sides represent the two elementary steps in the evolution of the lattice Boltzmann equation: advection and collision. The advection process is naturally executed in velocity space $\mathbb{V}$, $f_\alpha(\boldsymbol{r}_i,t)$ being simply shifted in space according to the velocity $\boldsymbol{e}_\alpha$ to $f_\alpha(\boldsymbol{r}_i+\boldsymbol{e}_\alpha\delta t, t+\delta t)$. The collision process is naturally accomplished in the space spanned by the eigenvectors of the collision matrix, the corresponding eigenvalues being the inverse of their relaxation time towards their equilibria. The $(N+1)$ eigenvalues of S are all between 0 and 2 so as to maintain linear stability and the separation of scales, which means that the relaxation times of non-conserved quantities are much faster than the hydrodynamic time-scales. The LBGK models are special cases in which the $(N+1)$ relaxation times are all equal, and the collision matrix $\mathsf{S} = \omega\mathsf{I}$, where I is the identity matrix, $\omega = 1/\tau$, and τ $(> 1/2)$ is the single relaxation time of the model.

To simulate athermal fluids, a necessary criterion is that the discrete velocity set must be sufficient to represent a scalar (mass density ρ), a vector (momentum $\boldsymbol{j}$), another scalar (pressure P), and a symmetric traceless second-rank tensor (viscous stress tensor σ_{ij}). More generally, the velocity set must possess sufficient symmetries for the hydrodynamic equations to hold: the conserved quantities and their fluxes must transform properly so that they can approximate their continuous counterparts in an appropriate limit. Finally, the local conserved quantities must be the mass density ρ and the momentum $\boldsymbol{j}$ for athermal fluids.

Given a chosen set of discrete velocities $\{\boldsymbol{e}_\alpha \mid \alpha = 0,1,\ldots,N\}$ and corresponding distribution functions $\{f_\alpha \mid \alpha = 0,1,\ldots,N\}$, an equal number of moments $\{m_\beta \mid \beta = 0,1,\ldots,N\}$ of the distribution functions f_α can be obtained as

$$m_\beta \equiv \langle\phi_\beta|f\rangle = \langle f|\phi_\beta\rangle, \qquad \langle f| = (f_0, f_1, \ldots, f_N), \tag{2.2}$$

where $\{|\phi_\beta\rangle|\beta = 0,1,\ldots,N\}$ is an orthogonal dual basis set constructed by the Gram–Schmidt orthogonalization procedure (see, for example, Bouzidi *et al.* 2001*a*) from polynomials of the column vectors $|e_{x_i}\rangle$ in space $\mathbb{V}$. Vector $|e_{x_i}\rangle$ is built from the components of the $\boldsymbol{e}_\alpha$, i.e. $|e_{x_i}\rangle \equiv (e_{0x_i}, e_{1x_i}, \ldots, e_{Nx_i})^{\mathrm{T}}$, for $i \in \{1,2,\ldots,D\}$ in D dimensions (e.g. $\{|e_x\rangle, |e_y\rangle, |e_z\rangle\}$ in three dimensions).

The set $\{|\phi_\beta\rangle\}$ is analogous to the Hermite tensor polynomials in continuous velocity space (Grad 1958; Harris 1971). It should be stressed that the orthogonal functions defined on a finite set of discrete velocities $\{\boldsymbol{e}_\alpha\}$ has some degeneracies which do not exist in the Hermite tensor polynomials in continuous space. Obviously, the moments are simply linear combinations of the f_α, therefore velocity space $\mathbb{V}$, spanned by $|f\rangle \equiv (f_0, f_1, \ldots, f_N)^{\mathrm{T}}$, and the moment space $\mathbb{M}$, spanned by $|m\rangle \equiv (m_0, m_1, \ldots, m_N)^{\mathrm{T}}$, are related by a linear mapping M: $|m\rangle = \mathsf{M}|f\rangle$ and $|f\rangle = \mathsf{M}^{-1}|m\rangle$. The transformation matrix M would be an orthogonal transformation if the basis vectors $\{|\phi_\beta\rangle\}$ are normalized.

If the matrix S is chosen such that the $\{|\phi_\beta\rangle\}$ are its eigenvectors, the linear relaxation of the kinetic modes in moment space $\mathbb{M}$ naturally accomplishes the collision process. Then the evolution equation (2.1) of the MRT lattice Boltzmann equation becomes (d'Humières 1992; Lallemand & Luo 2000):

$$|f(\boldsymbol{r}_i + \boldsymbol{e}_\alpha \delta t, t + \delta t)\rangle - |f(\boldsymbol{r}_i, t)\rangle = -\mathsf{M}^{-1}\hat{\mathsf{S}}[|m(\boldsymbol{r}_i, t)\rangle - |m^{(\mathrm{eq})}(\boldsymbol{r}_i, t)\rangle], \tag{2.3}$$

where the collision matrix $\hat{\mathsf{S}} = \mathsf{M} \cdot \mathsf{S} \cdot \mathsf{M}^{-1}$ is diagonal: $\hat{\mathsf{S}} \equiv \mathrm{diag}(s_0, s_1, \ldots, s_N)$, and $m_\alpha^{(\mathrm{eq})}$ is the equilibrium value of the moment m_α. The $(N+1)$ moments can be separated into two groups: the 'hydrodynamic' (conserved) moments and the 'kinetic' (non-conserved) moments. The first group consists of the moments locally conserved in the collision process, so that in general $m_\beta^{(\mathrm{eq})} = m_\beta$. The second group consists of the moments not conserved in the collision process so that $m_\beta^{(\mathrm{eq})} \neq m_\beta$. The equilibria $\{m_\beta^{(\mathrm{eq})}\}$ are functions of the conserved moments and are invariant under the symmetry group of the underlying lattice. For models designed to simulate athermal fluids, the only hydrodynamic moments are mass density ρ (a scalar) and momentum $\boldsymbol{j}$ (a vector): energy is not a conserved quantity for athermal fluids. Equilibrium values of kinetic moments are functions of ρ and $\|\boldsymbol{j}\|^2$ for scalars, and $\boldsymbol{j}$ times some functions of ρ and $\|\boldsymbol{j}\|^2$ (eventually a constant) for vectors, and so on, as discussed in § 3.

From the above definition of the conserved and non-conserved moments, equation (2.3) can be rewritten as

$$|f(\boldsymbol{r}_i + \boldsymbol{e}_\alpha \delta t, t + \delta t)\rangle - |f(\boldsymbol{r}_i, t)\rangle = -\sum_{\beta \in B^{(\mathrm{K})}} \frac{s_\beta}{\langle \phi_\beta | \phi_\beta \rangle}[(m_\beta(\boldsymbol{r}_i, t) - m_\beta^{(\mathrm{eq})}(\boldsymbol{r}_i, t))]|\phi_\beta\rangle, \tag{2.4}$$

where we have used the fact that $(\mathsf{M} \cdot \mathsf{M}^{\mathrm{T}})$ is a diagonal matrix with diagonal elements $\langle \phi_\beta | \phi_\beta \rangle$. It is obvious that the actual values of the s_β for conserved moments are irrelevant, because $m_\beta^{(\mathrm{eq})}(\boldsymbol{r}_i, t) = m_\beta(\boldsymbol{r}_i, t)$ for $\beta \in B^{(\mathrm{H})}$ by definition, but they are set to zero in general in what follows. Note that this point is purely academic in the present context, but is very important when including body forces, as shown by Ginzbourg & Adler (1994).

The RLBE formulation has two important consequences. First, one has the maximum number of adjustable relaxation times, one for each class of kinetic modes invariant under the symmetry group of the underlying lattice. Second, one has maximum freedom in the construction of the equilibrium functions of the non-conserved moments. One immediate result of using the RLBE instead of the LBGK model is a significant improvement in numerical stability (Lallemand & Luo 2000). It should be emphasized that the above procedures are general and are independent of the number of discrete velocities and the number of space dimensions.

3. Multiple-relaxation-time D3Q15 model

Each point on a unit cubic lattice space has six nearest neighbours, $(\pm 1, 0, 0)$, $(0, \pm 1, 0)$, and $(0, 0, \pm 1)$, twelve next nearest neighbours, $(\pm 1, \pm 1, 0)$, $(\pm 1, 0, \pm 1)$, and $(0, \pm 1, \pm 1)$, and eight third nearest neighbours, $(\pm 1, \pm 1, \pm 1)$. Elementary discrete velocity sets for lattice Boltzmann models in three dimensions are constructed from the set of 26 vectors pointing from the origin to the above neighbours and the zero vector $(0, 0, 0)$. The 27 velocities are usually grouped into four subsets labelled

by their squared modulus, 0, 1, 2, and 3. We also use the notation DdQq for the q-velocity model in d-dimensional space in what follows (Qian *et al*. 1992). The D3Q15 model uses the velocity subsets 0, 1, and 3 and is described here as an example. The D3Q19 model uses the subsets 0, 1, and 2 and is described in the appendix. The D3Q13 model introduced by d'Humières *et al*. (2001) only uses the subsets 0 and 2.

The 15 discrete velocities in the D3Q15 model are

$$\boldsymbol{e}_\alpha = \begin{cases} (0,0,0), & \alpha = 0, \\ (\pm 1,0,0),(0,\pm 1,0),(0,0,\pm 1), & \alpha = 1,2,\ldots,6, \\ (\pm 1,\pm 1,\pm 1), & \alpha = 7,8,\ldots,14. \end{cases} \tag{3.1}$$

The components of the corresponding 15 orthogonal basis vectors $|\phi_\beta\rangle_\alpha$ are given by

$$\left.\begin{aligned} |\phi_0\rangle_\alpha &= \|\boldsymbol{e}_\alpha\|^0, \\ |\phi_1\rangle_\alpha &= \|\boldsymbol{e}_\alpha\|^2 - 2, \\ |\phi_2\rangle_\alpha &= \tfrac{1}{2}(15\|\boldsymbol{e}_\alpha\|^4 - 55\|\boldsymbol{e}_\alpha\|^2 + 32), \end{aligned}\right\} \tag{3.2}$$

$$\left.\begin{aligned} |\phi_3\rangle_\alpha &= e_{\alpha x}, \\ |\phi_5\rangle_\alpha &= e_{\alpha y}, \\ |\phi_7\rangle_\alpha &= e_{\alpha z}, \end{aligned}\right\} \tag{3.3}$$

$$\left.\begin{aligned} |\phi_4\rangle_\alpha &= \tfrac{1}{2}(5\|\boldsymbol{e}_\alpha\|^2 - 13)e_{\alpha x}, \\ |\phi_6\rangle_\alpha &= \tfrac{1}{2}(5\|\boldsymbol{e}_\alpha\|^2 - 13)e_{\alpha y}, \\ |\phi_8\rangle_\alpha &= \tfrac{1}{2}(5\|\boldsymbol{e}_\alpha\|^2 - 13)e_{\alpha z}, \end{aligned}\right\} \tag{3.4}$$

$$\left.\begin{aligned} |\phi_9\rangle_\alpha &= 3e_{\alpha x}^2 - \|\boldsymbol{e}_\alpha\|^2, \\ |\phi_{10}\rangle_\alpha &= e_{\alpha y}^2 - e_{\alpha z}^2, \end{aligned}\right\} \tag{3.5}$$

$$\left.\begin{aligned} |\phi_{11}\rangle_\alpha &= e_{\alpha x}e_{\alpha y}, \\ |\phi_{12}\rangle_\alpha &= e_{\alpha y}e_{\alpha z}, \\ |\phi_{13}\rangle_\alpha &= e_{\alpha x}e_{\alpha z}, \end{aligned}\right\} \tag{3.6}$$

$$|\phi_{14}\rangle_\alpha = e_{\alpha x}e_{\alpha y}e_{\alpha z}, \tag{3.7}$$

where $\alpha \in \{0,1,\ldots,14\}$, $\|\boldsymbol{e}_\alpha\| = (e_{\alpha x}^2 + e_{\alpha y}^2 + e_{\alpha z}^2)^{1/2}$ and $\|\boldsymbol{e}_0\|^0 = 1$. The orthogonal basis set $\{|\phi_\beta\rangle\}$ is obtained by orthogonalizing the polynomials of the column vectors $|e_{x_i}\rangle$ by the standard Gram–Schmidt procedure (see, for example, Bouzidi *et al*. 2001*a*). The corresponding 15 moments $\{m_\beta \mid \beta = 0,1,\ldots,14\}$ are the mass density ($m_0 = \rho$), the part of the kinetic energy independent of the density ($m_1 = e$), the part of the kinetic energy square independent of the density and kinetic energy ($m_2 = \varepsilon = e^2$), the momentum ($m_{3,5,7} = j_{x,y,z}$), the energy flux independent of the mass flux ($m_{4,6,8} = q_{x,y,z}$), the symmetric traceless viscous stress tensor ($m_9 = 3p_{xx}$, $m_{10} = p_{ww} = p_{yy} - p_{zz}$, with $p_{xx} + p_{yy} + p_{zz} = 0$, $m_{11,12,13} = p_{xy,yz,zx}$), and an antisymmetric third-order moment ($m_{14} = m_{xyz}$), corresponding to the following order:

$$|m\rangle = (\rho, e, \varepsilon, j_x, q_x, j_y, q_y, j_z, q_z, 3p_{xx}, p_{ww}, p_{xy}, p_{yz}, p_{zx}, m_{xyz})^{\mathrm{T}}.$$

The collision matrix $\hat{S}$ in moment space $\mathbb{M}$ is the diagonal matrix

$$\hat{S} \equiv \mathrm{diag}(0, s_1, s_2, 0, s_4, 0, s_4, 0, s_4, s_9, s_9, s_{11}, s_{11}, s_{11}, s_{14}), \tag{3.8}$$

zeros corresponding to conserved moments in the order chosen. And the matrix M is then given by

$$\begin{vmatrix}
1 & 1 & 1 & 1 & 1 & 1 & 1 & 1 & 1 & 1 & 1 & 1 & 1 & 1 & 1 \\
-2 & -1 & -1 & -1 & -1 & -1 & -1 & 1 & 1 & 1 & 1 & 1 & 1 & 1 & 1 \\
16 & -4 & -4 & -4 & -4 & -4 & -4 & 1 & 1 & 1 & 1 & 1 & 1 & 1 & 1 \\
0 & 1 & -1 & 0 & 0 & 0 & 0 & 1 & -1 & 1 & -1 & 1 & -1 & 1 & -1 \\
0 & -4 & 4 & 0 & 0 & 0 & 0 & 1 & -1 & 1 & -1 & 1 & -1 & 1 & -1 \\
0 & 0 & 0 & 1 & -1 & 0 & 0 & 1 & 1 & -1 & -1 & 1 & 1 & -1 & -1 \\
0 & 0 & 0 & -4 & 4 & 0 & 0 & 1 & 1 & -1 & -1 & 1 & 1 & -1 & -1 \\
0 & 0 & 0 & 0 & 0 & 1 & -1 & 1 & 1 & 1 & 1 & -1 & -1 & -1 & -1 \\
0 & 0 & 0 & 0 & 0 & -4 & 4 & 1 & 1 & 1 & 1 & -1 & -1 & -1 & -1 \\
0 & 2 & 2 & -1 & -1 & -1 & -1 & 0 & 0 & 0 & 0 & 0 & 0 & 0 & 0 \\
0 & 0 & 0 & 1 & 1 & -1 & -1 & 0 & 0 & 0 & 0 & 0 & 0 & 0 & 0 \\
0 & 0 & 0 & 0 & 0 & 0 & 0 & 1 & -1 & -1 & 1 & 1 & -1 & -1 & 1 \\
0 & 0 & 0 & 0 & 0 & 0 & 0 & 1 & 1 & -1 & -1 & -1 & -1 & 1 & 1 \\
0 & 0 & 0 & 0 & 0 & 0 & 0 & 1 & -1 & 1 & -1 & -1 & 1 & -1 & 1 \\
0 & 0 & 0 & 0 & 0 & 0 & 0 & 1 & -1 & -1 & 1 & -1 & 1 & 1 & -1
\end{vmatrix}. \tag{3.8}$$

Note that the row vectors of M, $\{\langle\phi_\beta|\}$, are orthogonal to each other but they are not normalized, i.e. $\langle\phi_\alpha|\phi_\beta\rangle = \|\phi_\alpha\| \cdot \|\phi_\beta\| \cdot \delta_{\alpha\beta}$. Note also that, with different ordering and normalization, the basis vectors $\{|\phi_k\rangle\}$ given by Ginzburg (2001) are the same as the ones given here, except $|\phi_1\rangle$ and $|\phi_2\rangle$ which are replaced by an orthogonal linear combination. This would make a difference only when $s_1 \neq s_2$. The 4th, 6th, and 8th row vectors of M (corresponding to j_x, j_y, and j_z, respectively) uniquely define the ordering (or labelling) of the velocity set $\{\boldsymbol{e}_\alpha\}$ in subscript α.

With $c_s^2 = 1/3$ (c_s is the sound speed) and $s_9 = s_{11}$, the equilibria of the kinetic moments as of $\rho^{(eq)} = \rho$ and $\boldsymbol{j}^{(eq)} = \boldsymbol{j}$ up to second order are given by

$$e^{(eq)} = -\rho + \frac{1}{\rho_0}\boldsymbol{j}\cdot\boldsymbol{j} = -\rho + \frac{1}{\rho_0}(j_x^2 + j_y^2 + j_z^2), \tag{3.9}$$

$$\varepsilon^{(eq)} = -\rho, \tag{3.10}$$

$$q_x^{(eq)} = -\tfrac{7}{3}j_x, \qquad q_y^{(eq)} = -\tfrac{7}{3}j_y, \qquad q_z^{(eq)} = -\tfrac{7}{3}j_z, \tag{3.11}$$

$$p_{xx}^{(eq)} = \frac{1}{3\rho_0}[2j_x^2 - (j_y^2 + j_z^2)], \qquad p_{ww}^{(eq)} = \frac{1}{\rho_0}[j_y^2 - j_z^2], \tag{3.12}$$

$$p_{xy}^{(eq)} = \frac{1}{\rho_0}j_x j_y, \qquad p_{yz}^{(eq)} = \frac{1}{\rho_0}j_y j_z, \qquad p_{xz}^{(eq)} = \frac{1}{\rho_0}j_x j_z, \tag{3.13}$$

$$m_{xyz}^{(eq)} = 0. \tag{3.14}$$

The constants are defined as follows. The constant ρ_0 is the mean density in the system and is usually set to be unity in simulations. The approximation of $1/\rho \approx 1/\rho_0$ is used in equations (3.9), (3.12) and (3.13) to reduce compressibility effects in the model (He & Luo 1997*c*). If the usual compressible Navier–Stokes equations are required, one only has to replace ρ_0 by ρ. Equation (3.10) has the general form $\varepsilon^{(eq)} = w_\varepsilon\rho + w_{\varepsilon j}\boldsymbol{j}\cdot\boldsymbol{j}/\rho_0$, where w_ε and $w_{\varepsilon j}$ are free parameters which do not have much effect on the asymptotic Navier–Stokes equation simulated by the model. In this model, we set $w_\varepsilon = -1$ and $w_{\varepsilon j} = 0$; to recover the LBGK model, one must set $w_\varepsilon = 1$ and $w_{\varepsilon j} = -5$.

The above equilibrium functions are obtained by optimizing the isotropy and Galilean invariance of the model. The details are described in Lallemand & Luo (2000). The kinematic viscosity ν and the bulk viscosity ζ of the model are

$$\nu = \frac{1}{3}\left(\frac{1}{s_9} - \frac{1}{2}\right) = \frac{1}{3}\left(\frac{1}{s_{11}} - \frac{1}{2}\right), \tag{3.15}$$

$$\zeta = \frac{(5 - 9c_s^2)}{9}\left(\frac{1}{s_1} - \frac{1}{2}\right) = \frac{2}{9}\left(\frac{1}{s_1} - \frac{1}{2}\right). \tag{3.16}$$

We emphasize that the above formulae are obtained under the conditions that $s_9 = s_{11}$ and $\boldsymbol{q}^{(\mathrm{eq})}$ of equation (3.11), which are the results of the optimization, and the mean fluid velocity $\boldsymbol{V} = \boldsymbol{0}$. Corrections to these transport coefficients for finite $\boldsymbol{k}$ and non-zero mean velocity $\boldsymbol{V}$ can be calculated from the solution of the linearized dispersion equation of the system, which is equivalent to the standard von Neumann stability analysis (Lallemand & Luo 2000).

Some properties of the lattice Boltzmann equation are dictated by the symmetries of the discrete velocity set and the simplicity of the dynamics on the lattice. One consequence is the existence of spurious invariants that may lead to some undesirable artefacts in simulations, especially near boundaries. One such invariant is the staggered invariant in LGA and LBE models (Zanetti 1989). The D3Q15 model has also another special invariant not found in most LBE models: the parity $\chi(\boldsymbol{r}_i)$ of a vector $\boldsymbol{r}_i = (x_i, y_i, z_i)$ defined on a three-dimensional cubic lattice by

$$\chi(\boldsymbol{r}_i) = (x_i + y_i + z_i) \pmod 2, \quad \text{for } \boldsymbol{r}_i \in \mathbb{Z}^3. \tag{3.17}$$

For the D3Q15 model, if $\chi(\boldsymbol{r}_i)$ is 0 ($\boldsymbol{r}_i \in \mathbb{Z}_{\mathrm{e}}^3$), then $\chi(\boldsymbol{r}_i + \boldsymbol{e}_\alpha)$ is 1 ($\boldsymbol{r}_i \in \mathbb{Z}_{\mathrm{o}}^3$) for $\boldsymbol{e}_\alpha \neq \boldsymbol{0}$, and vice versa. This means that the system has two decoupled sub-lattices ($\mathbb{Z}_{\mathrm{o}}^3$ and $\mathbb{Z}_{\mathrm{e}}^3$) for momentum, and these two sub-lattices can be coupled through boundary conditions. Consequently, the system has a checkerboard (parity) invariance and one should be aware of this fact when using the D3Q15 models, especially when short-wavelength oscillations are observed in simulations. The oscillations due to the checkerboard invariance often cause numerical instability in simulations. In contrast, the D3Q19 model with velocities of parities 0 and 1 does not have this checkerboard invariance.

4. Simulations

In order to demonstrate the enhanced stability of the RLBE approach, we simulated a diagonally lid-driven cavity flow (Povitsky 2001) with a flow configuration shown in figure 1. The mesh is uniform and of size 52^3. The boundary condition (BC) at the top plane (at $y = 1$) is $\boldsymbol{U}_{\mathrm{BC}} = -(\sqrt{2}, 0, \sqrt{2})/20$, so that $U_{\mathrm{BC}} = \|\boldsymbol{U}_{\mathrm{BC}}\| = 0.1$ in lattice units. The other five planes were subject to no-slip boundary conditions.

The relaxation parameters used in the RLBE simulations are $\rho_0 = 1$, $s_1 = 1.6$, $s_2 = 1.2$, $s_4 = 1.6$ and $s_{14} = 1.2$. The values of the relaxation parameters (s_α) and the adjustable parameters in $\varepsilon^{(\mathrm{eq})}$ (w_ε and $w_{\varepsilon j}$) have been obtained to attain optimal numerical stability but can only be regarded as 'sub-optimal' values which are the result of a compromise between the expected range for the Reynolds number and the effort required to find the optimal values by searching a large parameter space through *linear* analysis. These parameters are not adjusted to the actual Reynolds

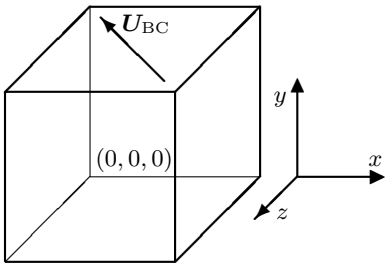

Figure 1. Diagonally driven cavity flow.

number in each simulation, but are kept constant once chosen. The relaxation parameters $s_9 = s_{11}$ are determined by the viscosity from equation (3.15). The accuracy of the simulation is also enhanced by using, instead of the variable ρ, its fluctuations $\delta\rho \equiv \rho - \rho_0$.

The boundary conditions on the top plane are obtained in velocity space by assigning distributions to (Ladd 1994)

$$f_\alpha = w_\alpha \rho_0 \frac{\boldsymbol{e}_\alpha \cdot \boldsymbol{U}_{\mathrm{BC}}}{c_{\mathrm{s}}^2}, \tag{4.1}$$

where $w_\alpha = 1/9$ for $\alpha \in \{1, \ldots, 6\}$ and $w_\alpha = 1/72$ for $\alpha \in \{7, \ldots, 14\}$. It should be stressed that this particular implementation of a sliding boundary imposes a constant pressure $p_0 = c_{\mathrm{s}}^2 \rho_0$ at the boundary, which is incorrect; and the momentum transfer in the direction perpendicular to the moving lid is significantly weakened. The correct boundary conditions consistent with the bounce-back boundary conditions should be (Luo 1998, 2000; Bouzidi *et al*. 2001*b*)

$$f_{\bar{\alpha}} = f_\alpha + 2w_\alpha \rho_0 \frac{\boldsymbol{e}_{\bar{\alpha}} \cdot \boldsymbol{U}_{\mathrm{BC}}}{c_{\mathrm{s}}^2} = f_\alpha - 2w_\alpha \rho_0 \frac{\boldsymbol{e}_\alpha \cdot \boldsymbol{U}_{\mathrm{BC}}}{c_{\mathrm{s}}^2}, \tag{4.2}$$

where $f_{\bar{\alpha}}$ is the distribution function of $\bar{\boldsymbol{e}}_\alpha \equiv -\boldsymbol{e}_\alpha$. Nevertheless, the implementation prescribed by equation (4.1) does help to enhance the stability of the D3Q15 model. The 'node' bounce-back boundary conditions are applied to the rest five walls for no-slip boundary conditions (Cornubert *et al*. 1991). The 'node' bounce-back boundary conditions differ from the 'link' bounce-back boundary conditions by a one-step delay in time but otherwise they are the same. This one-time-step delay seems to effectively reduce oscillations caused by the parity invariance and thus enhances the numerical stability (Cornubert 1991).

As the effective width of the system is approximately 50 lattice units, the Reynolds number $Re = 50U_{\mathrm{BC}}/\nu$ was set by varying the viscosity ν. We computed the lower bounds of the viscosity for this particular flow by using the RLBE and LBGK schemes. The lower bounds are 0.6×10^{-3} for the RLBE scheme and 2.5×10^{-3} for the LBGK scheme with identical discretization, initial and boundary conditions. Viscosities smaller than these bounds would lead to numerical instability in the simulation. Hence for our test problem with the same mesh size, the maximum Reynolds number attainable by using the RLBE scheme is about four times that attainable using the LBGK scheme.

For the Povitsky cavity flow (Povitsky 2001) at a low Reynolds number, $Re = 500$, (viscosity $\nu = 0.01$), the pressure field computed by the LBGK scheme shows severe

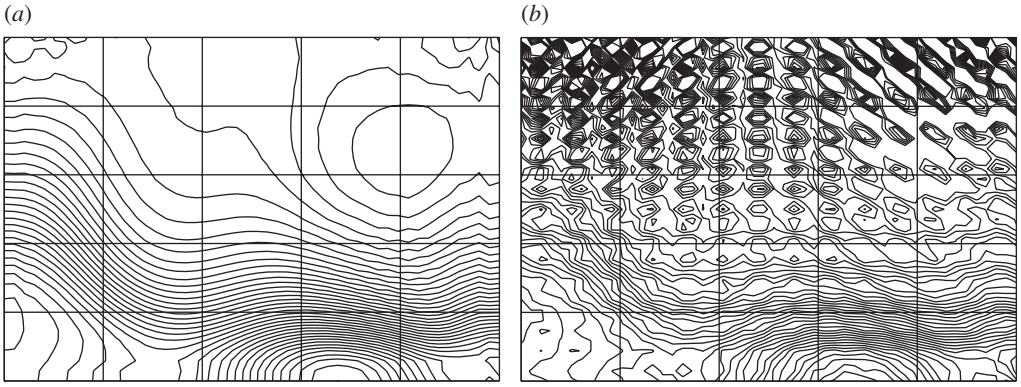

Figure 2. Cavity flow $Re = 500$ pressure contours at $z = 0.5$: (*a*) RLBE, (*b*) LBGK.

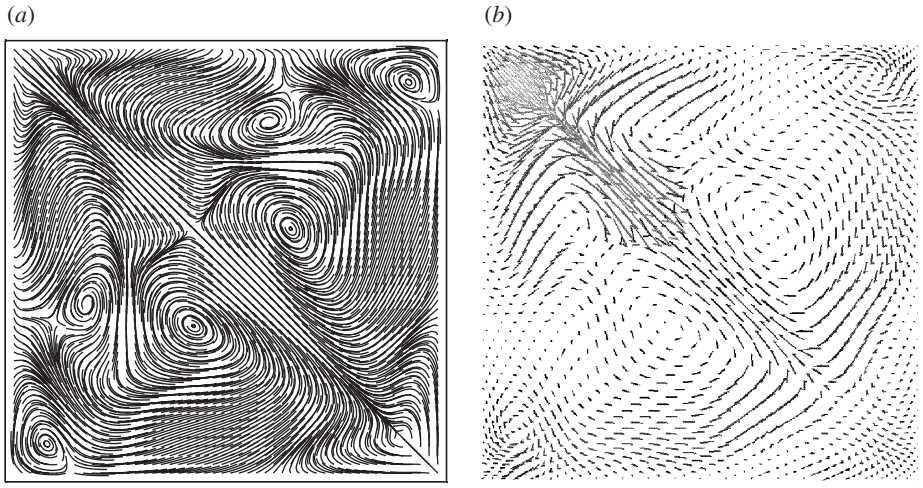

Figure 3. Cavity flow $Re = 2000$ stream lines at $y = 0.5$: (*a*) RLBE, (*b*) FLUENT.

oscillations throughout the entire computational domain, even in locations far away from the corner singularities, in contrast to the much smoother pressure field obtained by using the RLBE scheme, as depicted in figure 2.

When the Reynolds number is increased to 2000, the solution obtained by using the RLBE scheme agrees reasonably well with that obtained by using the commercial software FLUENT with a *non-uniform* 68^3 mesh (Povitsky 2001), as shown in figure 3, even though the RLBE grid resolution is much coarser. At a relatively high grid Reynolds number $Re^* \equiv U/\nu = 40$, the pressure field still bears useful information, at least at some distance from the top corner singularities, as shown in figure 4. In contrast, the LBGK simulation at $Re = 2000$ did not converge due to severe oscillations. With further increase of the Reynolds number to 4000 ($\nu = 0.001\,25$), the flow field becomes unsteady and complex three-dimensional vortex shedding are observed. Detailed analysis of the flow will be published elsewhere.

In the simulations, suitable coding techniques should be applied to optimize the computational efficiency of the code. First and foremost, one should not use matrix calculations in the transformations between space $\mathbb{V}$ and space $\mathbb{M}$, instead, the trans-

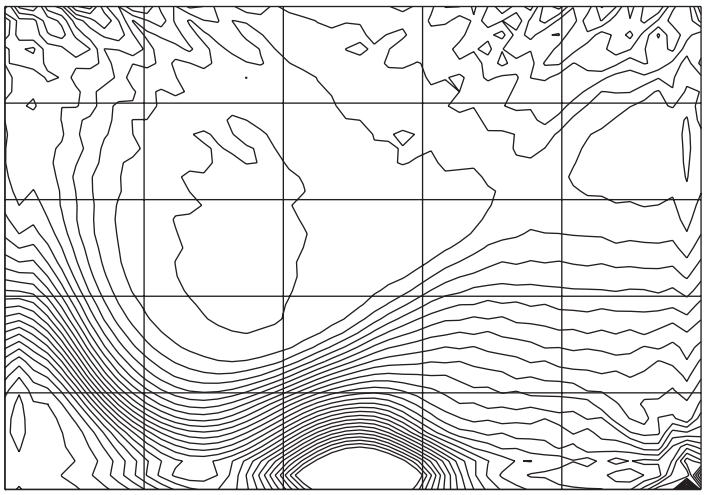

Figure 4. Cavity flow $Re = 2000$ pressure contours at $z = 0.5$, RLBE 52^3 uniform grids.

formations should be carried out explicitly using the formulae mapping $|f\rangle$ to $|m\rangle$ and vice versa (equations (2.2) and (2.4)). Secondly, the equilibria must be computed in moment space $\mathbb{M}$ and not in velocity space $\mathbb{V}$: this is the reason why we do not provide the equilibrium distribution functions $f_\alpha^{(\mathrm{eq})}$. Thirdly, all the common sub-expressions should be computed only once. This can be achieved either by explicitly computing these sub-expressions as separate variables or by carefully putting them between parentheses and trusting modern compilers to do the sub-expression reduction themselves. Various compiler optimization options can easily accomplish this. Finally, the use of $\rho_0 = 1$ instead of ρ avoids the need for a division in the calculations of the equilibria, and the use of $\delta\rho$ instead of ρ to increase numerical accuracy.

By following these basic practices based on common sense, the number of operations required for the simulation of the MRT D3Q15 model can be reduced to less than 120 additions/subtractions and 40 multiplications per time-step on a grid point, as opposed to 80 additions/subtractions and 40 multiplications for the LBGK scheme with the same optimization effort. (The purpose of this counting is not to find the exact lower bounds, but only to have an estimate.) We would also like to stress that on modern computers the computational performance of lattice Boltzmann schemes is mostly limited by the available memory bandwidth and that rather soon the cost of local floating-point operations will be negligible. For instance, combining the collision and propagation steps into one loop would reduce about one-third of the time, because use of two loops doubles the memory access time. (However, this combination of loops is difficult to implement on vector machines.) With the optimization except the combination of collision and propagation together, the number of sites updated per second of the RLBE D3Q15 scheme for our test carried out on one node (eight processors) of a Hitachi SR-8000 parallel vector machine is about 1.76×10^7 as opposed to 2.06×10^7 for the LBGK D3Q15 scheme: the RLBE scheme is *ca.* 17% slower than the LBGK counterpart. The achieved FLOPS rate is 3.18 GFLOPS for the RLBE scheme versus 2.70 GFLOPS for the LBGK scheme. However, it is important to note that, with the same computational effort and near the limit of numerical stability, the results obtained by using the RLBE scheme are much more accurate

than the results obtained by using the LBGK scheme, which are contaminated by numerical instability.

Free of the parity invariance, the D3Q19 RLBE model (see the appendix) further improves the stability. We have tested the D3Q19 RLBE model in the Povitsky cavity flow (Povitsky 2001). We used the 'link' bounce-back boundary conditions for the five walls and the correct boundary condition of equation (4.2) for the moving lid. With the same resolution of 51^3, the results obtained by using the D3Q19 RLBE model are much more accurate than those obtained by using the D3Q15 RLBE model with different boundary conditions. This confirms the previous observation that the D3Q19 LBGK model is more stable than the D3Q15 LBGK model (Mei *et al*. 2000). A further comparative study of these two RLBE models is left for future work.

5. Conclusions

In this paper we provide a synopsis of the MRT LBE in three dimensions and demonstrate its superior numerical stability and efficiency through the simulation of the diagonally lid-driven cavity flow in three dimensions. The flow is geometrically simple, steady, and yet non-trivial. For this flow we estimate that the improvement in stability brought by the RLBE scheme yields about a four-fold gain in maximum Reynolds number when compared with the LBGK scheme. Of course, this improvement would be flow and boundary and initial condition dependent. Given that the computational effort required to solve time-dependent flows in three dimensions is basically proportional to Re^3, the stability improvement by using the RLBE scheme would reduce the computational effort by *at least* one order of magnitude while maintaining the accuracy of the simulations.

We are grateful to Dr R. Rubinstein for his careful reading of the manuscript. M.K. acknowledges the technical support from the Leibniz-Rechenzentrum München. L.S.L. is partly supported by the United States Air Force Office for Scientific Research under grant no. F49620-01-1-0142 (technical monitor Dr J. Tishkoff).

Appendix A. Multiple-relaxation-time D3Q19 model

The 19 discrete velocities in D3Q19 models are

$$\boldsymbol{e}_\alpha = \begin{cases} (0,0,0), & \alpha = 0, \\ (\pm 1,0,0), \quad (0,\pm 1,0), \quad (0,0,\pm 1), & \alpha = 1,2,\ldots,6, \\ (\pm 1,\pm 1,0), \quad (\pm 1,0,\pm 1), \quad (0,\pm 1,\pm 1), & \alpha = 7,8,\ldots,18, \end{cases} \tag{A 1}$$

and the components of the 19 orthogonal basis vectors are given by

$$\left.\begin{aligned} |\phi_0\rangle_\alpha &= \|\boldsymbol{e}_\alpha\|^0, \\ |\phi_1\rangle_\alpha &= 19\|\boldsymbol{e}_\alpha\|^2 - 30, \\ |\phi_2\rangle_\alpha &= (21\|\boldsymbol{e}_\alpha\|^4 - 53\|\boldsymbol{e}_\alpha\|^2 + 24)/2, \end{aligned}\right\} \tag{A 2}$$

$$\left.\begin{aligned} |\phi_3\rangle_\alpha &= e_{\alpha x}, \\ |\phi_5\rangle_\alpha &= e_{\alpha y}, \\ |\phi_7\rangle_\alpha &= e_{\alpha z}, \end{aligned}\right\} \tag{A 3}$$

$$\left.\begin{aligned} |\phi_4\rangle_\alpha &= (5\|\boldsymbol{e}_\alpha\|^2 - 9)e_{\alpha x},\\ |\phi_6\rangle_\alpha &= (5\|\boldsymbol{e}_\alpha\|^2 - 9)e_{\alpha y},\\ |\phi_8\rangle_\alpha &= (5\|\boldsymbol{e}_\alpha\|^2 - 9)e_{\alpha z}, \end{aligned}\right\} \tag{A 4}$$

$$\left.\begin{aligned} |\phi_9\rangle_\alpha &= 3e_{\alpha x}^2 - \|\boldsymbol{e}_\alpha\|^2,\\ |\phi_{11}\rangle_\alpha &= e_{\alpha y}^2 - e_{\alpha z}^2, \end{aligned}\right\} \tag{A 5}$$

$$\left.\begin{aligned} |\phi_{13}\rangle_\alpha &= e_{\alpha x}e_{\alpha y},\\ |\phi_{14}\rangle_\alpha &= e_{\alpha y}e_{\alpha z},\\ |\phi_{15}\rangle_\alpha &= e_{\alpha x}e_{\alpha z}, \end{aligned}\right\} \tag{A 6}$$

$$\left.\begin{aligned} |\phi_{10}\rangle_\alpha &= (3\|\boldsymbol{e}_\alpha\|^2 - 5)(3e_{\alpha x}^2 - \|\boldsymbol{e}_\alpha\|^2),\\ |\phi_{12}\rangle_\alpha &= (3\|\boldsymbol{e}_\alpha\|^2 - 5)(e_{\alpha y}^2 - e_{\alpha z}^2), \end{aligned}\right\} \tag{A 7}$$

$$\left.\begin{aligned} |\phi_{16}\rangle_\alpha &= (e_{\alpha y}^2 - e_{\alpha z}^2)e_{\alpha x},\\ |\phi_{17}\rangle_\alpha &= (e_{\alpha z}^2 - e_{\alpha x}^2)e_{\alpha y},\\ |\phi_{18}\rangle_\alpha &= (e_{\alpha x}^2 - e_{\alpha y}^2)e_{\alpha z}, \end{aligned}\right\} \tag{A 8}$$

where $\alpha \in \{0, 1, \ldots, 18\}$. The corresponding 19 moments $\{m_\beta \mid \beta = 0, 1, \ldots, 18\}$ are arranged in the following order:

$$|m\rangle = (\rho, e, \varepsilon, j_x, q_x, j_y, q_y, j_z, q_z, 3p_{xx}, 3\pi_{xx}, p_{ww}, \pi_{ww}, p_{xy}, p_{yz}, p_{xz}, m_x, m_y, m_z)^{\mathrm{T}}.$$

There are 14 vectors in the orthogonal basis set $\{|\phi_\beta\rangle\}$ with the same physical significance of the basis vectors in the D3Q15 model except for $|\phi_{14}\rangle$. These 14 vectors correspond to the following moments: ρ, e, ε, $\boldsymbol{j}$, $\boldsymbol{q}$, and p_{ij}. In the D3Q19 basis set $\{|\phi_\beta\rangle\}$ there is no vector corresponding to the moment m_{xyz} of equation (3.7). Instead, there are five vectors which are not in the D3Q15 basis set: three vectors of cubic order ($|\phi_{16}\rangle$, $|\phi_{17}\rangle$, and $|\phi_{18}\rangle$) and two of quartic order ($|\phi_{10}\rangle$ and $|\phi_{12}\rangle$). These five vectors are polynomials in $|\phi_3\rangle$, $|\phi_5\rangle$ and $|\phi_7\rangle$. The two vectors of quartic order, $|\phi_{10}\rangle$ and $\phi_{12}\rangle$, have the same symmetry as the diagonal part of the traceless tensor p_{ij}, while the other three vectors of cubic order are parts of a third rank tensor, with the symmetry of $j_k p_{nm}$.

The diagonal collision matrix $\hat{\boldsymbol{S}}$ is

$$\hat{\boldsymbol{S}} \equiv \mathrm{diag}(0, s_1, s_2, 0, s_4, 0, s_4, 0, s_4, s_9, s_{10}, s_9, s_{10}, s_{13}, s_{13}, s_{13}, s_{16}, s_{16}, s_{16}),$$

and the transformation matrix $\boldsymbol{M}$ is given by the matrix opposite.

Again, the 4th, 6th and 8th row vectors of $\boldsymbol{M}$ (corresponding to j_x, j_y, and j_z, respectively) uniquely define the ordering (or labelling) of the velocity set $\{\boldsymbol{e}_\alpha\}$ with respect to subscript α.

With $c_{\mathrm{s}}^2 = 1/3$ and $s_9 = s_{13}$, the equilibria of the non-conserved moments are given as functions up to second-order in ρ and $\boldsymbol{j}$ as follows:

$$e^{(\mathrm{eq})} = -11\rho + \frac{19}{\rho_0}\boldsymbol{j}\cdot\boldsymbol{j} = -11\rho + \frac{19}{\rho_0}(j_x^2 + j_y^2 + j_z^2), \tag{A 9}$$

$$\varepsilon^{(\mathrm{eq})} = w_\varepsilon\rho + \frac{w_{\varepsilon j}}{\rho_0}\boldsymbol{j}\cdot\boldsymbol{j}, \tag{A 10}$$

$$q_x^{(\mathrm{eq})} = -\tfrac{2}{3}j_x, \qquad q_y^{(\mathrm{eq})} = -\tfrac{2}{3}j_y, \qquad q_z^{(\mathrm{eq})} = -\tfrac{2}{3}j_z, \tag{A 11}$$

1	1	8	1	0	0	−1	−1	−1	−1	−2	−2	0	0	0	1	0	0	−1	1
1	1	8	1	0	0	1	1	−1	−1	−2	−2	0	0	0	−1	0	0	1	1
1	1	8	1	0	0	−1	−1	1	1	−2	−2	0	0	0	−1	0	0	−1	−1
1	1	8	1	0	0	1	1	1	1	−2	−2	0	0	0	1	0	0	1	−1
1	1	8	1	−1	−1	0	0	−1	−1	1	1	−1	−1	0	0	1	1	−1	−1
1	1	8	1	1	1	0	0	−1	−1	1	1	−1	−1	0	0	−1	−1	0	0
1	1	8	1	−1	−1	0	0	1	1	1	1	−1	−1	0	0	1	1	0	0
1	1	8	1	1	1	0	0	1	1	1	1	−1	−1	0	0	−1	−1	0	0
1	1	8	1	−1	−1	0	0	0	0	0	0	1	1	0	0	1	1	0	0
1	1	8	1	−1	−1	0	0	0	0	0	0	1	1	0	0	−1	−1	0	0
1	1	8	1	1	1	0	0	0	0	0	0	1	1	0	0	−1	−1	0	0
1	1	8	1	−1	−1	0	0	0	0	0	0	1	1	0	0	1	1	0	0
1	1	8	1	1	1	0	0	0	0	0	0	1	1	0	0	−1	−1	0	0
1	1	8	1	0	0	1	−1	0	0	0	0	1	1	0	0	0	0	1	−1
1	1	−11	−4	0	0	0	0	−1	4	−1	2	−1	2	0	0	0	0	0	0
1	1	−11	−4	0	0	0	0	1	−4	−1	2	−1	2	0	0	0	0	0	0
1	1	−11	−4	0	0	−1	4	0	0	−1	2	1	−2	0	0	0	0	0	0
1	1	−11	−4	0	0	1	−4	0	0	−1	2	1	−2	0	0	0	0	0	0
1	1	−11	−4	−1	4	0	0	0	0	2	−4	0	0	0	0	0	0	0	0
1	1	−11	−4	1	−4	0	0	0	0	−4	0	0	0	0	0	0	0	0	0
1	−30	12	0	0	0	0	0	0	0	0	0	0	0	0	0	0	0	0	0

$$p_{xx}^{(\mathrm{eq})} = \frac{1}{3\rho_0}[2j_x^2 - (j_y^2 + j_z^2)], \qquad p_{ww}^{(\mathrm{eq})} = \frac{1}{\rho_0}[j_y^2 - j_z^2], \tag{A 12}$$

$$p_{xy}^{(\mathrm{eq})} = \frac{1}{\rho_0} j_x j_y, \qquad p_{yz}^{(\mathrm{eq})} = \frac{1}{\rho_0} j_y j_z, \qquad p_{xz}^{(\mathrm{eq})} = \frac{1}{\rho_0} j_x j_z, \tag{A 13}$$

$$\pi_{xx}^{(\mathrm{eq})} = w_{xx} p_{xx}^{(\mathrm{eq})}, \qquad \pi_{ww}^{(\mathrm{eq})} = w_{xx} p_{ww}^{(\mathrm{eq})}, \tag{A 14}$$

$$m_x^{(\mathrm{eq})} = m_y^{(\mathrm{eq})} = m_z^{(\mathrm{eq})} = 0, \tag{A 15}$$

where w_ε and $w_{\varepsilon j}$ are again free parameters and w_{xx} is an additional free parameter in the D3Q19 model.

The bulk viscosity ζ of the D3Q19 model is equal to that of the D3Q15 model given in equation (3.16) and its kinematic viscosity ν is

$$\nu = \frac{1}{3}\left(\frac{1}{s_9} - \frac{1}{2}\right) = \frac{1}{3}\left(\frac{1}{s_{13}} - \frac{1}{2}\right). \tag{A 16}$$

To recover the corresponding LBGK model, one must set $w_\varepsilon = 3$, $w_{\varepsilon j} = -11/2$, and $w_{xx} = -1/2$. However, to attain an optimized stability of the model, we obtained the following parameter values through linear analysis (Lallemand & Luo 2000): $w_\varepsilon = 0$, $w_{\varepsilon j} = -475/63$, $w_{xx} = 0$, $s_1 = 1.19$, $s_2 = s_{10} = 1.4$, $s_4 = 1.2$, and $s_{16} = 1.98$. With the above parameter values, we can use a maximum speed of 0.19 (Mach number $M \approx 0.33$) and a viscosity $\nu > 2.54 \times 10^{-3}$ in simulations. The linear analysis to obtain these 'optimal' parameter values is a local analysis of a system with a uniform velocity of wave-vector $\boldsymbol{k}$. The local analysis does not consider boundary conditions and therefore the system may be less stable in actual simulations.

References

Bhatnagar, P. L., Gross, E. P. & Krook, M. 1954 A model for collision processes in gases. I. Small amplitude processes in charged and neutral one-component systems. *Phys. Rev.* **94**, 511–525.

Bouzidi, M., d'Humières, D., Lallemand, P. & Luo, L.-S. 2001*a* Lattice Boltzmann equation on a two-dimensional rectangular grid. *J. Computat. Phys.* **172**, 704–717.

Bouzidi, M., Firdaouss, M. & Lallemand, P. 2001*b* Momentum transfer of a Boltzmann-lattice fluid with boundaries. *Phys. Fluids* **13**, 3452–3459.

Chen, H., Chen, S. & Matthaeus, W. H. 1992 Recovery of the Navier–Stokes equations using a lattice gas Boltzmann method. *Phys. Rev.* A **45**, R5339–R5342.

Cornubert, R. 1991 Conditions aux limites des modèles cinétiques discrets: Couche de Knudsen et obstacles. PhD thesis, Université Pierre et Marie Curie, Paris.

Cornubert, R., d'Humières, D. & Levermore, D. 1991 A Knudsen layer theory for lattice gases. *Physica* D **47**, 241–259.

d'Humières, D. 1992 Generalized lattice Boltzmann equations. In *Rarefied gas dynamics: theory and simulations* (ed. B. D. Shizgal & D. P. Weaver). *Prog. Aeronaut. Astronaut.* **159**, 450–458.

d'Humières, D., Bouzidi, M. & Lallemand, P. 2001 Thirteen-velocity three-dimensional lattice Boltzmann model. *Phys. Rev.* E **63**, 066702-1-7.

Ginzbourg, I. & Adler, P. M. 1994 Boundary flow condition analysis for the three-dimensional lattice Boltzmann model. *J. Physique II France* **4**, 191–214.

Ginzbourg, I. & Adler, P. 1995 Surface tension models with different viscosities. *Transport Porous Media* **20**, 37–76.

Ginzburg, I. 2001 Introduction of upwind and free boundary into lattice Boltzmann method. In *Discrete modelling and discrete algorithms in continuum mechanics* (ed. Th. Sonar & I. Thomas), pp. 97–110. Berlin: Logos.

Ginzburg, I. & Steiner, K. 2002 Free surface lattice Boltzmann method to model the filling of expanding cavities by Bingham fluids. *Phil. Trans. R. Soc. Lond.* A **360**, 453–466.

Giraud, L., d'Humières, D. & Lallemand, P. 1997 A lattice Boltzmann model for visco-elasticity. *Int. J. Mod. Phys.* C **8**, 805–815.

Giraud, L., d'Humières, D. & Lallemand, P. 1998 A lattice Boltzmann model for Jeffreys visco-elastic fluid. *Europhys. Lett.* **42**, 625–630.

Grad, H. 1958 Principles of the kinetic theory of gases. In *Encyclopedia of physics* (ed. S. Flügge), vol. 12 (*Thermodynamics of gases*), pp. 205–294. Springer.

Harris, S. 1971 *An introduction to the theory of the Boltzmann equation*. New York: Holt, Rinehart and Winston.

He, X. & Luo, L.-S. 1997*a* *A priori* derivation of the lattice Boltzmann equation. *Phys. Rev.* E **55**, R6333–R6336.

He, X. & Luo, L.-S. 1997*b* Theory of the lattice Boltzmann method: from the Boltzmann equation to the lattice Boltzmann equation. *Phys. Rev.* E **56**, 6811–6817.

He, X. & Luo, L.-S. 1997*c* Lattice Boltzmann model for the incompressible Navier–Stokes equation. *J. Stat. Phys.* **88**, 927–944.

Higuera, F. & Jiménez, J. 1989 Boltzmann approach to lattice gas simulations. *Europhys. Lett.* **9**, 663–668.

Higuera, F., Succi, S. & Benzi, R. 1989 Lattice gas dynamics with enhanced collisions. *Europhys. Lett.* **9**, 345–349.

Ladd, A. J. C. 1994 Numerical simulations of particulate suspensions via a discretized Boltzmann equation. I. Theoretical foundation. *J. Fluid Mech.* **271**, 285–309.

Lallemand, P. & Luo, L.-S. 2000 Theory of the lattice Boltzmann method: dispersion, dissipation, isotropy, Galilean invariance and stability. *Phys. Rev.* E **61**, 6546–6562.

Luo, L.-S. 1998 Unified theory of lattice Boltzmann models for nonideal gases. *Phys. Rev. Lett.* **81**, 1618–1621.

Luo, L.-S. 2000 Theory of the lattice Boltzmann method: lattice Boltzmann models for nonideal gases. *Phys. Rev.* E **62**, 4982–4996.

McNamara, G. R., Garcia, A. L. & Alder, B. J. 1995 Stabilization of thermal lattice Boltzmann models. *J. Stat. Phys.* **81**, 395–408.

Mei, R., Shyy, W., Yu, D. & Luo, L.-S. 2000 Lattice Boltzmann method for 3-D flows with curved boundary. *J. Computat. Phys.* **161**, 680–699.

Povitsky, A. 2001 High-incidence 3-D lid-driven cavity flow. American Institute of Aeronautics and Astronautics. AIAA Paper 01-2847, pp. 1–7.

Qian, Y., d'Humières, D. & Lallemand, P. 1992 Lattice BGK models for Navier–Stokes equation. *Europhys. Lett.* **17**, 479–484.

Zanetti, G. 1989 The hydrodynamics of lattice gas automata. *Phys. Rev.* A **40**, 1539–1548.